



1 Triple collocation validates CONUS-wide evapotranspiration inferred from atmospheric 2 conditions

3
4 Erica L. McCormick^{1,*}, Lillian E. Sanders¹, Kaighin A. McColl^{2,3}, Alexandra G. Konings¹

5 ¹ Department of Earth System Science, Stanford University

6
7 ² Department of Earth and Planetary Sciences, Harvard University

8 ³ School of Engineering and Applied Sciences, Harvard University

9 *Corresponding author: ericamcc@stanford.edu

10 Abstract

11 Large-scale estimation of evapotranspiration (ET) remains challenging because no direct remote
12 sensing estimates of ET exist and because most data-driven estimation approaches require
13 assumptions about the impact of moisture conditions and biogeography on ET. The surface flux
14 equilibrium (SFE) approach offers an alternative, deriving ET directly from atmospheric
15 temperature and humidity under the assumption that conditions in the atmospheric boundary
16 layer reflect ET's land boundary condition. We present a 4 km resolution, continental United
17 States-wide, daily ET dataset spanning from 1979 to 2024 using the SFE method. The Bowen
18 ratio is first calculated using the SFE method solely based on temperature and specific humidity
19 estimates from gridMET and then converted to ET using net radiation and ground heat fluxes
20 from ERA5-Land. We evaluate its performance using extended triple collocation to estimate the
21 standard deviation of the random error and the correlation coefficient of SFE ET compared to
22 true ET, as well as those of three widely used alternative ET datasets: GLEAM, FluxCom, and
23 ERA5-Land. Despite its extreme simplicity, SFE ET achieves performance comparable to or
24 exceeding the other datasets across large portions of CONUS, particularly in the Western U.S.,
25 while requiring no information about land surface, vegetation, or soil properties and no
26 assumptions about ET's response to environmental and climate drivers. Our results support the
27 use of SFE as a scalable, observation-driven method for estimating ET.

28 29 1. Introduction

30 Evapotranspiration (ET) dominates the terrestrial water cycle (Friedlingstein et al., 2019; Good
31 et al., 2015), controls the partitioning of radiation into latent and sensible heat (McColl and
32 Rigden, 2020), and plays a key role in driving the hydrologic cycle by returning water to the
33 atmosphere (Oki and Kanae, 2006). ET therefore has downstream feedbacks on temperature



34 (Teuling et al., 2010), precipitation, and vegetation productivity (Green et al., 2017) in addition
35 to directly impacting the carbon cycles through the trade-off between photosynthesis and
36 transpiration (Yang et al., 2023). However, estimation of ET via remote sensing remains a
37 significant challenge with implications for understanding of vegetation response to drought, fire
38 risk, and the accounting of freshwater resources.

39 One challenge for ET remote sensing is that, unlike some surface properties such as
40 temperature, we are unable to directly sense the flux of water or latent heat associated with ET
41 electromagnetically. Therefore, ET products must leverage modelling approaches - either
42 physical, hybrid, or machine learning - constrained by the data that *is* observable via remote
43 sensing. These modelling approaches for ET often assume - implicitly or explicitly - the response
44 of evaporation and transpiration to environmental drivers, such as drought or variations in land
45 cover.

46 Alternatively, surface flux equilibrium (SFE) is a data-driven method for estimating ET
47 directly from atmospheric conditions without relying on soil or vegetation parameterization.
48 The concept of surface flux equilibrium was first proposed by McColl et al. (2019) and states
49 that, under many circumstances, the atmosphere and land surface are coupled so that changes
50 in surface fluxes (including ET) are reflected in atmospheric temperature and humidity. This
51 approach has several advantages over other ET estimation methods. It requires no information
52 about vegetation, soil, or subsurface properties. It also makes no assumptions about root-zone
53 moisture status or vegetation response to water availability. This means it is well suited for
54 hydrological research attempting to interrogate the relationship between ET and water
55 availability or between ET and vegetation cover (or other biogeographic drivers). Additionally,
56 SFE includes no tunable parameters and can be computed easily using only three inputs - air
57 temperature, humidity, and net radiation - each of which is readily available at global scales
58 (McColl and Rigden, 2020).

59 However, more complex ET estimation methods would be expected to outperform SFE
60 in many settings due to its extreme simplicity and lack of adjustable parameters. Nevertheless,
61 previous SFE implementation and validation efforts indicate that SFE performance is
62 comparable - or even better than - other ET estimation methods at the point- and watershed-
63 scale (Chen et al., 2021; McColl and Rigden, 2020; Thakur et al., 2025). For example, SFE ET has
64 been found to be within the range of in situ measurement errors at a selection of inland eddy
65 covariance towers, an upper limit on the performance of any ET estimate (McColl and Rigden,
66 2020). Thakur et al. (2025) also calculated SFE ET at inland eddy covariance sites across the
67 continental United States (CONUS) using tower-based temperature, humidity, and net
68 radiation. They found that SFE ET outperformed remotely sensed ET from MODIS (Mu et al.,
69 2011) as well as from three ET algorithms using data from the ECOSystem Spaceborne Thermal



70 Radiometer Experiment on Space Station (ECOSTRESS): the Simplified Surface Energy Balance
 71 (Savoca et al., 2013) SSEBop, (Savoca et al., 2013), the atmosphere-land exchange inverse
 72 disaggregation algorithm (DisALEXI) and the Priestley-Taylor Jet Propulsion Laboratory model
 73 (PT-JPL, Fisher et al., 2020).

74 Thakur et al. (2025) further investigated the impact of input data on SFE performance by
 75 calculating SFE ET using three scenarios: only eddy covariance data, by using the North
 76 American Land Data Assimilation System (NLDAS, Xia et al., 2012) for temperature and humidity
 77 and the Clouds and the Earth's Radiant Energy System instrument (CERES, Doelling et al., 2013)
 78 for net radiation, and by finally using NLDAS for temperature and humidity and MODIS for net
 79 radiation. All three SFE ET implementations compared favorably to tower-based ET with R^2 of
 80 0.70, 0.68, and 0.67 for the tower-based SFE, CERES-based SFE, and MODIS-based SFE,
 81 respectively. This suggests that the emergent simplicity of ET that SFE takes advantage of is
 82 robust to choices of input data, at least at the scale of eddy covariance towers.

83 The only gridded estimates of SFE ET are reported by Chen et al. (2021), who calculated
 84 monthly ET at 0.125° across CONUS using net radiation from CERES and 2-m temperature and
 85 humidity from North American Regional Reanalysis (NARR, Mesinger et al., 2006). They
 86 compared SFE ET to estimates from the Coupled Model Intercomparison Project phase 6
 87 (CMIP6, Eyring et al., 2016) and to water balance-based ET estimates available at large
 88 catchments across CONUS. The error in the water balance-based estimates provides a minimum
 89 possible error, below which ET estimation approaches cannot be distinguished due to errors in
 90 the underlying reference data. They found that SFE ET errors are comparable to the error of the
 91 catchment water balances and that SFE outperforms the reanalysis (NARR) and most CMIP6
 92 models.

93 However, even this sole gridded implementation of SFE - while promising - is unable to
 94 provide a thorough evaluation of the SFE approach because the comparison datasets each have
 95 their own unquantified uncertainties. Therefore, disagreement between SFE and CMIP6 cannot
 96 be attributed to either dataset because their errors cannot be distinguished. One solution to
 97 this is the statistical evaluation approach of triple collocation. Using triple collocation and its
 98 updated counterpart, extended triple collocation (McColl et al., 2014), it is possible to compare
 99 three datasets with co-located measurements and estimate two important performance
 100 metrics: (1) the variability in the random error of each dataset and (2) the correlation between
 101 the measured value and the underlying 'true' variable. Both performance metrics can be
 102 calculated without reference to this unknowable 'true' variable, in this case ET, and without
 103 assuming the error of any of the three comparison datasets.



104 Triple collocation - sometimes also referred to as the ‘three-cornered hat’ approach -
 105 has been widely used in evaluating datasets where a ‘truth’ or reference dataset is unavailable,
 106 for example in the evaluation of datasets for soil moisture (Draper et al., 2013; Gruber et al.,
 107 2016; Scipal et al., 2008), ocean winds (Caires & Sterl, 2003), precipitation (Alemohammad et al,
 108 2015, Burnett et al 2020), sensible heat and carbon fluxes (Alemohammad et al, 2017), ET
 109 (Khan et al., 2018), near-surface air temperature and specific humidity (Sun et al., 2021), and
 110 terrestrial water storage (Ferreira et al., 2016). It can also be used to estimate the coupling of
 111 multiple variables, for example latent heat and soil moisture (Crow et al., 2015). Given three
 112 datasets with observations of the same state variable, each with their own non-correlated
 113 random errors, comparison of the three datasets via triple collocation enables calculation of
 114 each dataset’s random error variance (Stoffelen, 1998).

115 Here, we accomplish two steps in advancing the estimation of ET. First, we release the
 116 first publicly available, gridded dataset of daily SFE ET. We calculate this dataset at 4 km
 117 resolution across the continental United States (CONUS) using gridMET for 2-m temperature
 118 and humidity and net radiation from ERA5-Land. Second, we compare our gridded estimates of
 119 SFE ET to three other remotely sensed ET estimates: Global Land Evaporation Amsterdam
 120 Model Version 4 (GLEAM, Miralles et al., 2011), FluxCom (Jung et al., 2019), and ERA5-Land
 121 (Muñoz-Sabater et al., 2021). In addition to comparing the spatial pattern and variance of all
 122 datasets, we further use the statistical method of extended triple collocation following McColl
 123 et al. (2014) to calculate the error statistics of each dataset, despite lacking observations of
 124 ‘true’ ET (Gruber et al., 2016; McColl et al., 2014; Stoffelen, 1998).

125

126 **2. Methods**

127 ***2.1. Calculating ET from atmospheric conditions assuming surface flux equilibrium***

128 We calculate daily ET after McColl et al. (2019) by assuming that the near-surface atmosphere is
 129 in a state of ‘surface flux equilibrium’ where atmospheric conditions at the boundary layer
 130 reflect the recent fluxes of latent (λE) and sensible (H) heat on the Earth’s surface. If this is the
 131 case, then increasing ET (i.e. increasing latent heat) will correspond with diminished sensible
 132 heat and result in both atmospheric cooling and increased humidity. The ratio of sensible and
 133 latent heat fluxes - known as the Bowen ratio (B) - can therefore be approximated by
 134 temperature and humidity at the boundary layer, so long as atmospheric conditions reflect the
 135 integrated signal of fluxes on the Earth’s surface.

136

137 We use 2-m air temperature (T_a) and relative humidity (q_a) from gridMET (Abatzoglou,
 138 2013) to estimate the Bowen ratio, where $R_v = 461.5 \text{ (J kg}^{-1} \text{ K}^{-1})$ is the gas constant for water



139 vapor, $C_p = 1005 \text{ (J kg}^{-1} \text{ K}^{-1})$ is the specific heat capacity of air at constant pressure, and $\lambda = 2.56$
 140 $\times 10^6 \text{ (J kg}^{-1})$ is the latent heat of vaporization of water (Eq 1).

$$B = \frac{H}{\lambda E} \approx \frac{R_v c_p T_a^2}{\lambda^2 q_a} \quad \text{Eq. 1}$$

141 We choose gridMET due to its relatively fine spatial resolution of 4 km and its availability
 142 at the daily timescale across CONUS. Net radiation (R_n) allows conversion from the Bowen ratio
 143 to ET (Eq 2). We use R_n from ERA5-Land (Muñoz-Sabater et al., 2021) because of its high
 144 agreement with in situ measurements across CONUS (Yin et al., 2023). Additionally, we assume
 145 a ground heat flux (G) of 10%. We do not evaluate SFE ET on any days with negative R_n .

$$\lambda E = (1 + B)^{-1} (R_n - G) \quad \text{Eq. 2}$$

146

147 **2.2 Triple collocation error estimation**

148 Triple collocation assumes a linear error model for each dataset, where the observed value for
 149 a given dataset (x_i) is assumed to be a linear function of the “true” ET (T) obscured by a
 150 constant additive bias (α), a constant multiplicative bias (β) and a time-varying additive random
 151 error with zero mean (ϵ) (Eq 3).

$$x_i = \alpha_i + \beta_i T + \epsilon_i \quad \text{Eq. 3}$$

152

153 In addition to assuming a linear error model for each dataset, triple collocation further
 154 assumes that the errors of each dataset are stationary and uncorrelated both with each other
 155 and with the unknown truth (Gruber et al., 2016; McColl et al., 2014).

156 With these assumptions, the variance of each dataset (Q_{11}, Q_{22} , and Q_{33}) represents the
 157 sensitivity of the dataset to variations in the true signal (via the product of β_i and σ_T) plus the
 158 variance of the random error ($\sigma_{\epsilon_i}^2$) (Eq 4).

$$Q_{ii} = \sigma_{\epsilon_i}^2 = \beta_i^2 \sigma_T^2 + \sigma_{\epsilon_i}^2 \quad \text{Eq. 4}$$

159 Covariance between pairs of datasets (e.g. Q_{12}, Q_{13} , and Q_{23}) likewise provides
 160 information about each dataset’s sensitivity to the true unknown ET via β_i and σ_T . (Eq 5).

$$Q_{ij} = \sigma_{\epsilon_{ij}}^2 = \beta_i \beta_j \sigma_T^2 \quad \text{Eq. 5}$$



161 By treating the product of β_i and σ_T as a single unknown variable, the equations for the
 162 variance and covariance of each dataset and dataset pair result in six equations and six
 163 unknowns. These can be solved to calculate the standard deviation of the random error of each
 164 dataset, σ_ϵ (Eq 6).

$$\sigma_\epsilon = \begin{bmatrix} \sqrt{Q_{11} - \frac{Q_{12}Q_{13}}{Q_{23}}} \\ \sqrt{Q_{22} - \frac{Q_{12}Q_{23}}{Q_{13}}} \\ \sqrt{Q_{33} - \frac{Q_{13}Q_{23}}{Q_{12}}} \end{bmatrix} \quad \text{Eq. 6}$$

165 The absolute values of β_i cannot be separated from the absolute value of σ_T . However,
 166 many studies assume $\beta_i = 1$ for one dataset - effectively choosing it as a reference dataset
 167 which has no multiplicative bias - and calculate β_i for the other two datasets *relative* to the
 168 actual unknown multiplicative bias of the reference dataset. In this study, however, we do not
 169 separate β_i and σ_T .

170 Extended triple collocation further allows the calculation of the correlation between
 171 each dataset and the unknown truth, R_T , while requiring no additional information (McColl et
 172 al., 2014); Eq 7).

$$R_{T,i}^2 = \begin{bmatrix} \frac{Q_{12}Q_{13}}{Q_{11}Q_{23}} \\ \frac{Q_{12}Q_{23}}{Q_{22}Q_{13}} \\ \frac{Q_{13}Q_{23}}{Q_{33}Q_{12}} \end{bmatrix} \quad \text{Eq. 7}$$

173
 174 Triple collocation requires several assumptions, all of which are likely to be at least
 175 partially violated (e.g., Yilmaz and Crow, 2014). However, these assumptions are not unique to
 176 triple collocation. Gruber et al. (2016) showed that more common validation strategies
 177 implicitly require the same assumptions. For example, if we were to instead estimate the
 178 correlation coefficient and root-mean-squared error (RMSE) between SFE ET and another
 179 reference ET product, we would be implicitly making the same assumptions.

180 181 **2.3. Comparison ET datasets**

182 We compare SFE ET to ET from FluxCom, GLEAM version 4, and ERA5-Land. We compare all ET
 183 datasets over the years 1980 to 2016, which represents the maximum overlap in temporal
 184 coverage between all four datasets. Additionally, we resample each dataset to match the native



185 resolution of FluxCom at 0.5°. We match the FluxCom resolution because it is the coarsest. We
 186 choose to compare SFE to these particular three ET datasets not just because they are
 187 commonly used, but also to minimize violation of the triple collocation assumptions,
 188 particularly the assumption of independent errors between datasets. This is commonly
 189 achieved by using datasets that differ in their input data sources and modeling frameworks
 190 (Gruber et al., 2016; McColl et al., 2014). We also remove the seasonal cycle from each dataset
 191 by subtracting the 30-day rolling average from each day (Chen et al., 2018; Draper et al., 2013;
 192 Miralles et al., 2010). This ensures that differences in the seasonality and timing of ET do not
 193 impact the triple collocation analysis and has been shown to improve error estimation with
 194 triple collocation for ET datasets specifically (He et al., 2023). Finally, we use extended triple
 195 collocation to calculate the standard deviation of the random error and the correlation
 196 coefficient of each dataset (see Sec 2.2 above). Because we have four comparison datasets and
 197 triple collocation requires just three, we are able to repeat our estimates of each dataset's
 198 error statistics once for each possible 'triplet' (i.e. combination) of three datasets. Convergence
 199 of the error estimates regardless of the triplet chosen increases the robustness of the triple
 200 collocation assumptions and improves confidence in our calculated values (Draper et al., 2013;
 201 He et al., 2023). In addition to performing triple collocation, we also compare the four datasets
 202 via a general analysis of the variance and spatial patterns of ET.

203 The FluxCom dataset we choose for our triple collocation analysis uses machine learning
 204 to upscale eddy covariance measurements from flux towers based on satellite and
 205 meteorological inputs. FluxCom provides an ensemble of latent heat estimates trained using
 206 different meteorological datasets. In order to have the longest data record with daily
 207 resolution, here we use the single FluxCom ensemble member trained with the CRUNCEPv6
 208 reanalysis product (Wei et al., 2014), as opposed to the mean of all possible FluxCom ensemble
 209 members. However, the different model setups (each with a different weather model) were
 210 previously found to have similar performance (Jung et al., 2019). In addition to the climate data
 211 from CRUNCEP, FluxCom uses radiation data from CERES (Doelling et al., 2013), precipitation
 212 from the Global Precipitation Climatology Project (GPCP, Huffman et al., 2001), and
 213 temperature, land cover, and other reflectance indicators from MODIS. The FluxCom model is
 214 run per plant functional type and then combined into a single estimate by weighting each plant
 215 functional type's fractional areal coverage of the pixel (Jung et al., 2019).

216 GLEAM estimates ET by using remote sensing and reanalysis data to force a hybrid
 217 model which includes modules for canopy interception, potential evapotranspiration, soil water
 218 content, and vegetation response to evaporative stress. Although FluxCom and GLEAM have
 219 some remote sensing inputs in common, for example radiation from CERES and vegetation
 220 information from MODIS, GLEAM Version 4 takes a hybrid modelling approach and does not rely
 221 fully on machine learning like FluxCom. Specifically, GLEAM version 4 primarily uses physical



modelling modules with only a single module – for evaporative stress – using a deep neural network trained using in situ data from eddy covariance towers and sap flow measurements (Koppa et al., 2022; Martens et al., 2017; Miralles et al., 2025). This is in contrast to GLEAM version 3, which estimates evaporative stress empirically as a function of soil moisture and vegetation optical depth - both from microwave remote sensing inputs. Additionally, GLEAM Version 4 calculates ET using Penman’s equation (as opposed to Priestley-Taylor, used in Version 3) and also updates the multi-layer water balance model so that vegetation access to groundwater can be represented. However, in GLEAM Version 4, plant rooting depths are static for each land cover within the groundwater scheme and there is still a prescribed multiplicative stress function to determine how vegetation responds to soil moisture stress. GLEAM is the only dataset in our comparison set which partitions ET between evaporation, transpiration, and interception. We use the variable referring to the total evaporation (E) to best match the other ET estimates.

Finally, ERA5-Land uses the near-surface atmospheric reanalysis from ERA5, which assimilates observations from a range of satellites and in situ observation networks for many variables including land surface temperature, precipitation, wind speed, and soil moisture (Hersbach et al., 2020). ERA5-Land then takes the atmospheric states from ERA5 and re-runs the land surface model component at a finer resolution (9 km) offline (Muñoz-Sabater et al., 2021). This allows for additional and refined land surface parameterizations and corrections. Unlike FluxCom and GLEAM, ERA5-Land has no machine learning components. For our analysis, we sum the hourly latent heat flux output of ERA5-Land to daily totals and then resample bilinearly to match the coarser 0.5° FluxCom grid. Finally, both ERA5-Land and FluxCom report latent heat flux in units of energy per unit area, which we convert to ET (mm/day) by dividing by the latent heat of vaporization ($\lambda = 2.56 \times 10^6 \text{ J kg}^{-1}$).

246

2.4. Comparing performance across biogeographical factors

We compare the resulting σ_e and R_T estimates from triple collocation across a variety of biogeographical factors - specifically climate, elevation, land cover type, and the distance to the coast - to better understand under what conditions SFE ET performs well and how its performance across biogeography compares to that of the other ET estimates.

We calculate the mean annual precipitation at each pixel using monthly precipitation (P) from 1991 to 2020 from TerraClimate (Abatzoglou, 2013). We use elevation from MERIT Hydro (Version 1.0.1., (Yamazaki et al., 2019)). For land cover, we use the National Land Cover Database (NLCD) land cover map from 2021 (Dewitz, 2024). We consider the land cover types of forest (combining deciduous, evergreen, and mixed forests), shrub, grassland, wetland (combining woody and herbaceous wetlands), and agricultural (cultivated crops).



We further analyze the performance of each dataset by each pixel's distance from the coast because the assumptions of SFE are likely to be violated near the ocean (McColl et al., 2019). This is because in coastal regions, ocean moisture and temperature are expected to be a strong control on land surface fluxes. We calculate the distance of each pixel centroid from the nearest coast using the TIGER/Line Coastline National Shapefile (United States Census Bureau, 2019). We also exclude pixels from all analyses if their centroid overlaps with the ten largest water bodies in CONUS (ArcGIS Data and Maps, 2023).

265

266 **3. Results**

267 ***3.1. Surface flux equilibrium ET across CONUS from 1979 to 2024***

Here, we publicly release a dataset of daily SFE ET from 1979 to 2024 at 4 km resolution across CONUS (see Data Availability section). The spatial mean (shown in Figure 1a) follows expected patterns across CONUS - with an aridity driven gradient from West to East and a radiation driven gradient from North to South in the Eastern US. The temporal variability in daily ET calculated using the SFE approach is consistent with the comparison datasets (Figure S1). However, SFE has a larger standard deviation across much of CONUS - particularly the Western US - than FluxCom and GLEAM. Across several sample pixels, chosen as heavily vegetated examples spanning multiple regions, the seasonal cycle of mean annual ET is likewise comparable across all four ET estimates, although the timing of maximum summer ET each year varies between datasets (Figure 1b-g).

Although the magnitude of mean annual continental ET is most similar between SFE and FluxCom (Figure 2), the pattern of interannual variability which matches SFE the best is that of GLEAM ($\rho = 0.56$). The two datasets with the overall closest match in ET interannual variability, however, are FluxCom and ERA5-Land ($\rho = 0.71$). Although SFE and FluxCom each have intermediate magnitudes of mean continental ET relative to GLEAM and ERA5, both datasets - and FluxCom in particular - also have the lowest interannual variability magnitude (8 mm/year standard deviation for FluxCom and 12 mm/year for SFE, compared to 22 and 28 mm/year for ERA5-Land and GLEAM, respectively). Across the entire average record, the mean annual ET from SFE (598 mm/yr) sits roughly in the center of the four datasets, with GLEAM the lowest (555 mm/yr) and ERA5-Land the highest (641 mm/yr).

288

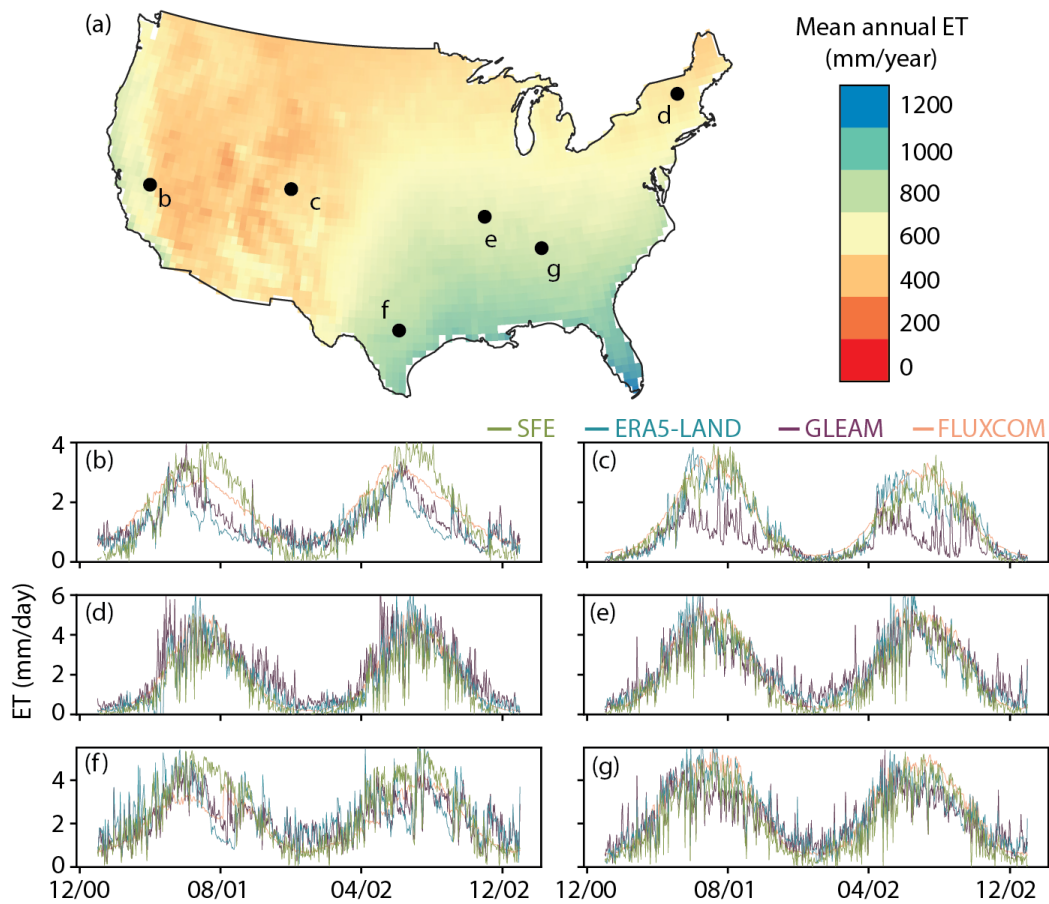


Figure 1. Mean annual SFE ET across CONUS from 1979 to 2024. Points show timeseries for example pixels for SFE (green), ERA5-Land (blue), GLEAM (purple) and FluxCom (pink).

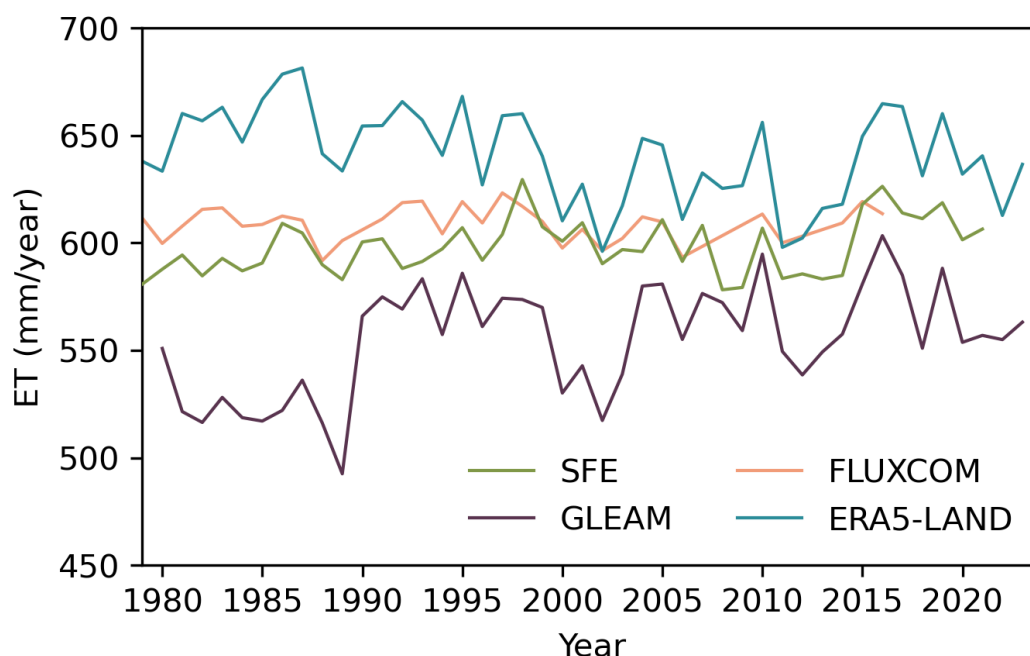


Figure 2. Interannual variability in mean annual ET across CONUS from 1979 through the record length of each dataset.

3.2. SFE is the only dataset that performs well in terms of both the standard deviation of the random error and the correlation coefficient

SFE performance as estimated by triple collocation is comparable - and even exceeds - the performance of the comparison datasets across much of CONUS, despite its extreme simplicity, lack of tunable parameters, and relatively small number of assumptions (Figure 3). SFE, FluxCom, and GLEAM show a strong divide in performance between the Western and Eastern US. SFE and FluxCom both have the lowest σ_ϵ and highest R_T in the Western US compared to the Eastern US. In contrast, GLEAM has lower σ_ϵ in the Western US, but higher R_T in the Eastern US. ERA5-Land shows more heterogeneity in performance across space - especially compared to SFE and FluxCom - and has no clear performance gradient between the Western and Eastern US.

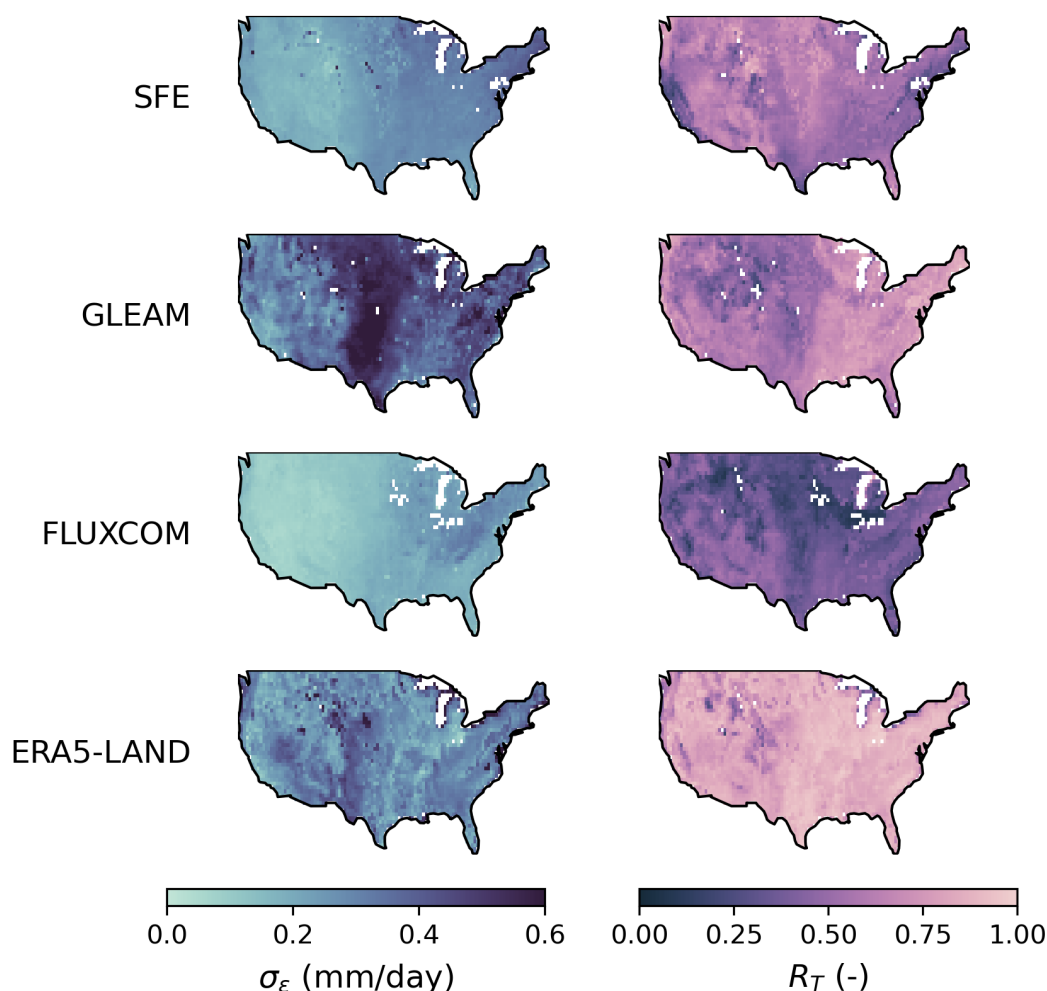


Figure 3. The standard deviation of the random error, σ_ϵ (left) and correlation coefficient to the truth, R_T (right) for each dataset averaged across all triplet combinations. Increasingly light colors are better performance. White pixels have no valid data for any triplet.

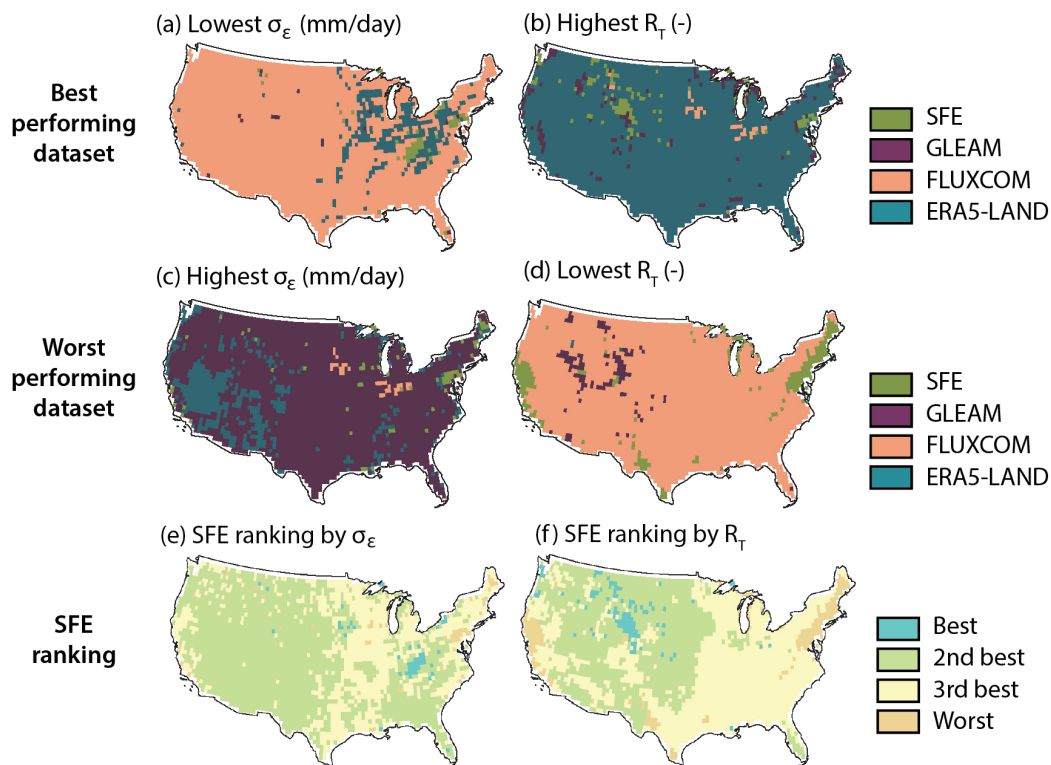
Despite its simplicity, SFE is the best or second-best dataset according to both σ_ϵ and R_T across more than half of CONUS (Figure 4). SFE has the lowest or second lowest σ_ϵ and highest or second highest R_T across 65.8% and 45.7% of pixels across CONUS, respectively (Figure 4, Table 1), mostly in the Western US.

SFE's high performance with regards to both σ_ϵ and R_T is unique among the comparison datasets. Other than SFE, the datasets with the best σ_ϵ and R_T , respectively, have the lowest



performance for the complementary metric. For example, FluxCom has the lowest σ_ϵ across the majority of CONUS, but it also has the lowest R_T (Figure 4). The opposite is true for ERA5, which is the highest performing dataset according to R_T across much of CONUS but frequently has the worst performance according to σ_ϵ , particularly in the US Southwest. SFE is the only dataset which consistently has high performance according to both metrics.

335
336



337
338

339 *Figure 4. Summary of relative performance of all four datasets. The dataset with highest*
340 *performance for the standard deviation of the random error, σ_ϵ (a) and the correlation*
341 *coefficient with ‘true’ ET, R_T (b) for each pixel. The worst performing datasets for σ_ϵ (c) and R_T*
342 *(d). The relative ranking of SFE for σ_ϵ (e) and R_T (f). The total number of pixels (and relative*
343 *percent of pixels) of each color are shown in Table 1. Pixels with centroids within 4 km (i.e., one*
344 *pixel) of the border have been removed.*
345



Table 1. (Top) The number of pixels where each dataset has the best performance according to the standard deviation of the random error, σ_ϵ , and the correlation coefficient to the truth, R_T . (Bottom) The number of pixels by SFE ET ranking.

Best dataset				
	By σ_ϵ		By R_T	
	Pixels	Percent	Pixels	Percent
SFE	58	(1.9%)	117	(3.9%)
GLEAM	17	(0.6%)	161	(5.3%)
FLUXCOM	2665	(87.9%)	34	(1.1%)
ERA5-Land	292	(9.6%)	2720	(89.7%)
Ranking of SFE				
	By σ_ϵ		By R_T	
	Pixels	Percent	Pixels	Percent
1st	48	(1.6%)	105	(3.5%)
2nd	1946	(64.2%)	1279	(42.2%)
3rd	975	(32.2%)	1455	(48.0%)
4th	63	(2.1%)	193	(6.4%)

We note that the estimates of σ_ϵ and R_T are consistent between triplets, indicating σ_ϵ and R_T estimates are robust to the choice of comparison datasets (Figure 5). Individual σ_ϵ and R_T maps for each dataset and triplet combination are shown in Figures S2 and S3. However, not all pixels have valid results for each triplet combination, which occurs when either σ_ϵ is negative for one or more of the datasets or if any R_T are greater than one. Figure 6 shows the total number of triplets which are valid for each pixel. The triplets with the most invalid pixels are those where FluxCom and ERA5-Land are both included. Invalid pixels are also more common in the Eastern US rather than the Western US. Even in the East, however, SFE - our main estimate of interest - still has at least one valid triplet in 96% of pixels and at least two valid triplets in 86% of pixels. SFE has three valid triplets - the maximum possible number for our four dataset analysis - in 55% of pixels.

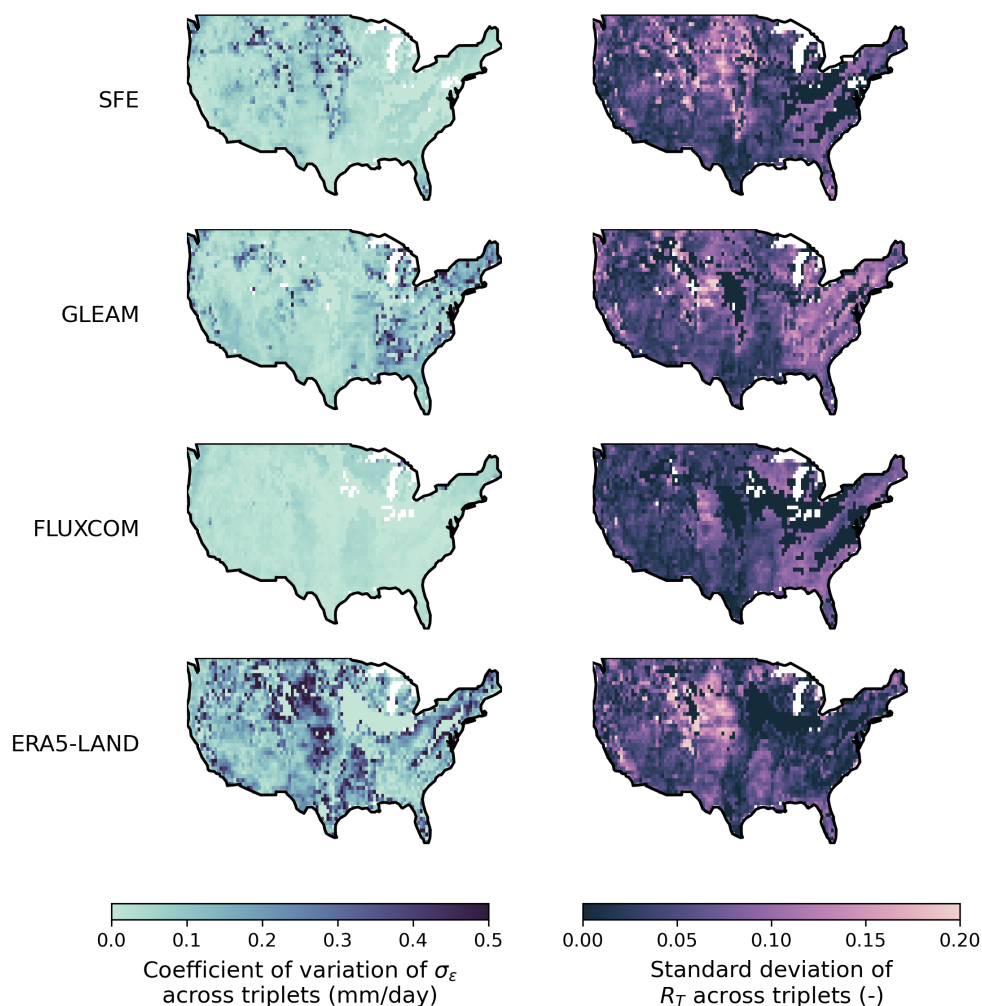


Figure 5. (left) The coefficient of variation of σ_ϵ for each dataset across all possible triplet combinations with valid data. White pixels have no valid data for any triplet. (right) The standard deviation of R_T for each dataset across all possible triplet combinations with valid data. White pixels have no valid data for any triplet and black pixels have only one triplet combination with valid data.

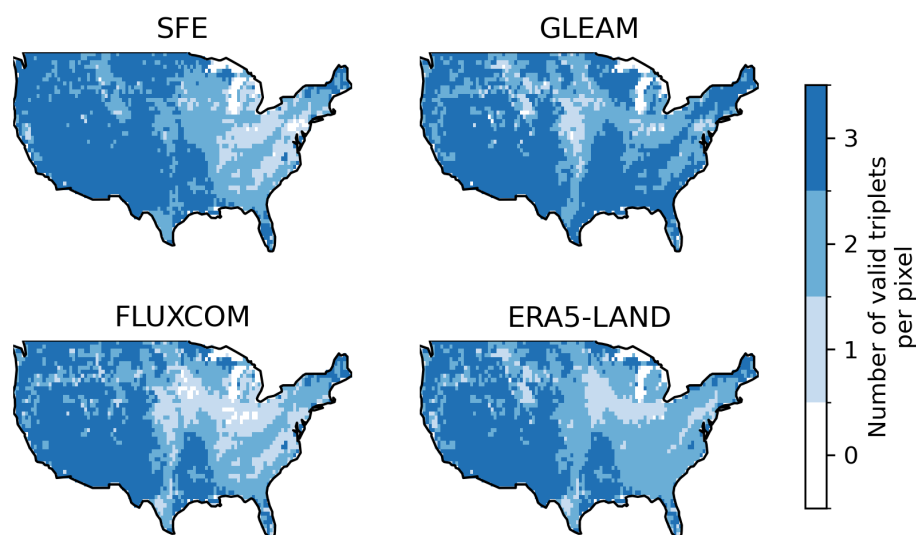


Figure 6. The total number of triple collocation estimates - one from each possible combination of datasets - that are averaged for each pixel and dataset combination. Pixels with no valid triple collocation results for any triplet are shown in white. The maximum number of valid triplets is three.

3.3. Performance across biogeographical factors

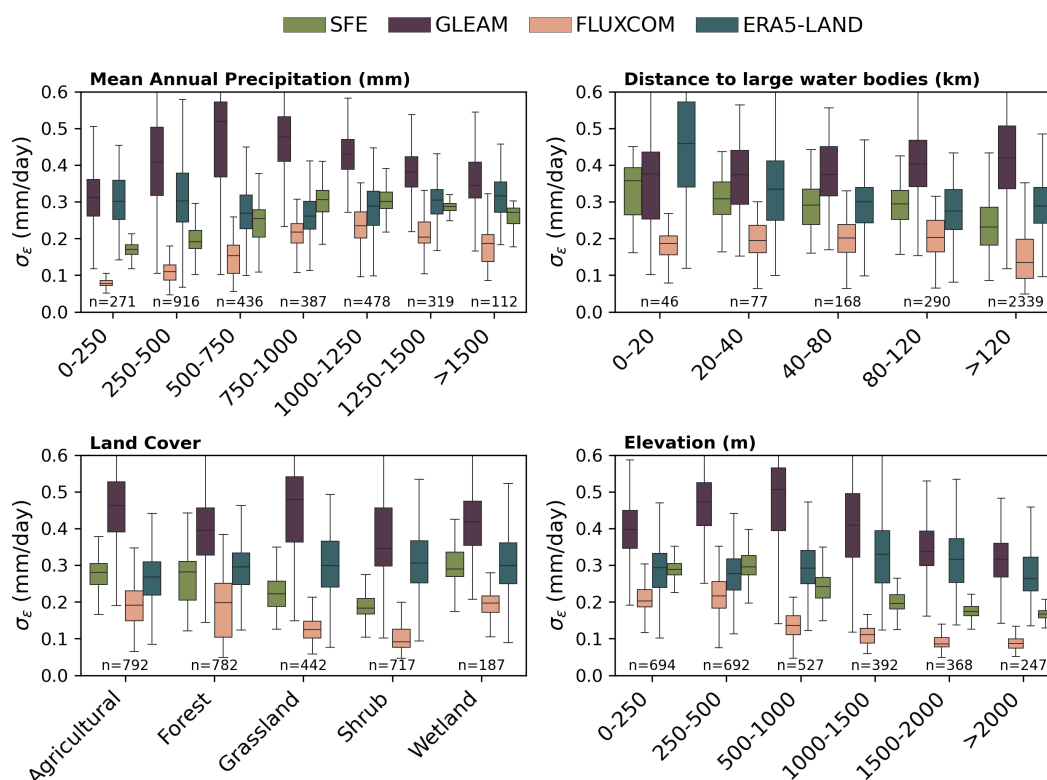
Comparing the trends of σ_ϵ (Figure 7) and R_T (Figure 8) across mean annual precipitation, elevation, landcover, and the distance to large water bodies shows that SFE performance is not more sensitive to any of these biogeographical factors than the comparison datasets. Even when comparing SFE performance with coastal proximity - a factor where we expect to see performance degradation due to the violation of SFE assumptions (McColl and Rigden, 2020) - the coastal proximity penalty of SFE is comparable to that of ERA5-Land. Indeed, ERA5-Land shows the sharpest decrease in performance within 20 km of the coast out of any of the datasets, however both SFE and ERA5-Land continue to show improved performance even up to 120 km inland. Neither GLEAM nor FluxCom have a strong relationship between coastal proximity and performance.

Likely due to its correlation with coastal proximity, SFE also has decreased performance at lower elevations with respect to both evaluation metrics. FluxCom and GLEAM likewise show their highest σ_ϵ at low elevations relative to higher elevations, with FluxCom σ_ϵ peaking around 500 m a.s.l. and GLEAM σ_ϵ around 1000 m. a.s.l. All three datasets continue to have decreased σ_ϵ as elevation increases. The relationship between elevation and R_T is relatively flat for SFE and FluxCom in the intermediate elevations, with the lowest R_T at the extreme low and high



elevations. GLEAM and ERA5, however, have continuously decreasing R_T with increasing elevation, and the lowest R_T at elevations exceeding 2000 m a.s.l.

409



410

411 *Figure 7. The standard deviation of the random error, σ_ϵ , for each ET dataset across mean*
 412 *annual precipitation, the distance to large water bodies, elevation, and land cover. The number*
 413 *of pixels in each category per ET dataset is shown below boxes.*

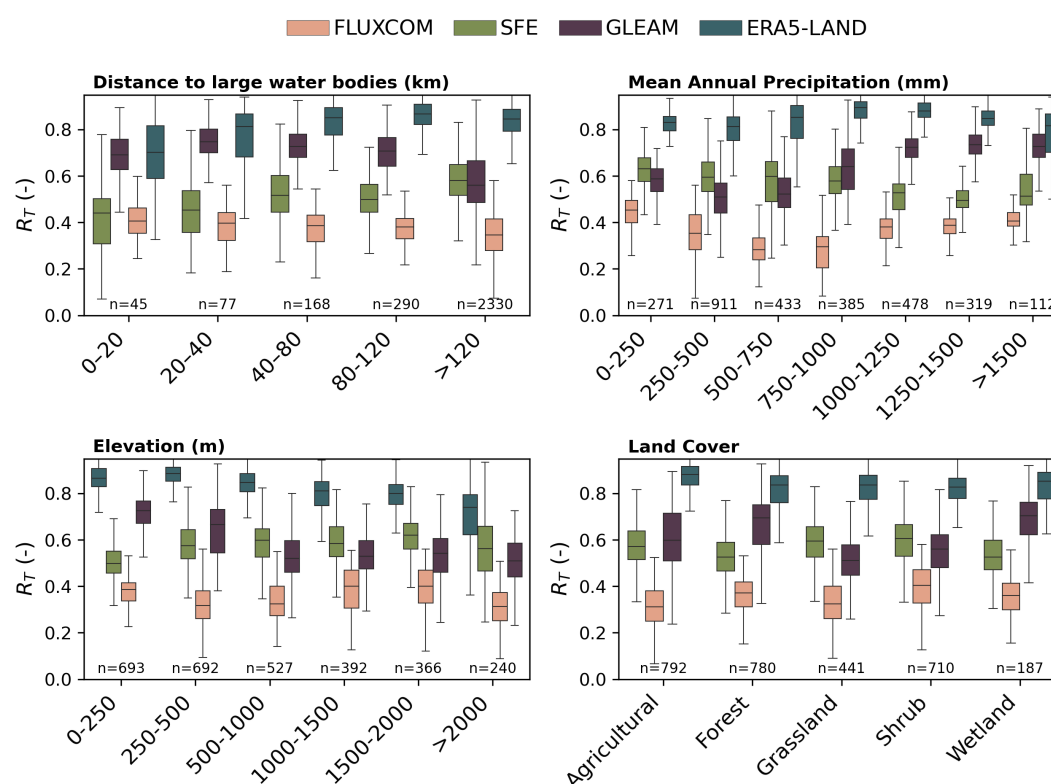
414

415 The σ_ϵ for SFE, GLEAM, and FluxCom is lowest at the driest and wettest pixels and
 416 highest at pixels with intermediate precipitation. However, the σ_ϵ for GLEAM peaks at the 500-
 417 750 mm/year bin whereas FluxCom and SFE have the highest σ_ϵ at slightly wetter locations,
 418 receiving between 1000-1250 mm/year. ERA5-Land, on the other hand, has a weaker
 419 relationship between MAP and σ_ϵ . ERA5-Land has the opposite pattern than the other datasets
 420 and shows the highest σ_ϵ at the driest and wettest pixels with lower σ_ϵ at intermediate aridity.
 421 The relationship between MAP and R_T follows that of MAP and σ_ϵ in general, however R_T does



not increase at the wettest pixels to the same degree as for the σ_e . For example, SFE has continually decreasing R_T as MAP increases with only a minimal increase in performance at the pixels with >1500 mm/year of precipitation.

425



426

427 *Figure 8. The correlation coefficient, R_T , for each ET dataset across mean annual precipitation,*
 428 *the distance to large water bodies, elevation, and land cover. The number of pixels in each*
 429 *category per ET dataset is shown below boxes.*

430

431 The performance variability across land cover is not consistent between any of the
 432 datasets. ERA5-Land has the lowest σ_e and highest R_T in agricultural pixels, GLEAM in forest
 433 pixels, and FluxCom in shrubland pixels. The SFE R_T is similar across all land cover types but SFE
 434 σ_e is highest in wetlands, followed by forest and agricultural pixels. Forested pixels also have a
 435 greater spread in σ_e for FluxCom and SFE compared to the other land cover types. SFE σ_e is
 436 lowest in shrublands, followed by grasslands. FluxCom σ_e is likewise lowest for grassland and



shrublands, which is the opposite of ERA5-Land, with the highest σ_ϵ in grasslands and shrublands.

439

4. Discussion

4.1. Which ET estimate is most accurate?

While triple collocation reveals that SFE is rarely the highest performing dataset, it is the second-best performing dataset across much of CONUS for both σ_ϵ and R_T (Figure 4e,f). In addition, we find that datasets which outperform SFE only exhibit better performance for one - not both - of either σ_ϵ and R_T . That SFE performs well - although not the best - for both metrics suggests its usefulness for a variety of applications, particularly those where it is not clear *a priori* whether having high R_T or low σ_ϵ is most useful. Furthermore, SFE may be a particularly good choice for studies interested in the response of ET to water limitations. Unlike the explicitly assumed dependence of ET on hydrologic conditions in ERA5-Land or the implicitly assumed dependence of GLEAM and FluxCom (which is limited by the constraints of the machine learning structure and input data), SFE contains no *a priori* assumptions about the effect of water stress on ET. Our release, alongside this manuscript, of a daily, 4km resolution CONUS-wide dataset of SFE-based ET spanning 1979 to 2024 should facilitate future applications of SFE for scientific analyses.

SFE is generally the second-best dataset regardless of metric, while alternative datasets with low random noise also have low correlation with the truth and vice versa. For example, across the four datasets tested, FluxCom has the lowest (most desirable) σ_ϵ across the majority of CONUS pixels (Figure 4a). However, it also has the lowest (least desirable) R_T more often than any other datasets (Figure 4d). ERA5-Land shows the converse relationship, with the highest (most desirable) R_T in almost all pixels compared to all other datasets, but poorer relative performance with regard to σ_ϵ (Figure 4b,c). How is this possible? To understand why, note that the triple collocation error model implies that,

$$R_{T,i}^2 = \frac{\beta_i^2 \sigma_T^2}{\beta_i^2 \sigma_T^2 + \sigma_{\epsilon,i}^2} \quad \text{Eq. 8}$$

as shown in McColl et al. (2014). For a dataset to exhibit both the lowest R_T and lowest σ_ϵ requires that β is also sufficiently small (σ_T is the same for each dataset and does not impact the ranking). An extreme example would be a dataset that simply set ET to a fixed climatological value and exhibited no temporal variability, for which $\beta = 0$ and $R_T = 0$, even when σ_ϵ is small. At the other extreme, for a dataset to exhibit both highest R_T and highest σ_ϵ requires β to be sufficiently large. In the limit of $\beta \rightarrow \infty$, $R_T = 1$, even when σ_ϵ is large. The relative importance of choosing a dataset with a low σ_ϵ , a high R_T , or a low bias (which is not



470 assessed here), depends on the application for which the ET dataset will be used (Entekhabi et
 471 al., 2010).

472 Beyond choosing a single dataset for a particular application, it is also possible to
 473 average multiple ET estimates into a single dataset weighted by each dataset's performance.
 474 While not often practical for large-scale use, He et al., (2023) used triple collocation to estimate
 475 an 'optimal' ET product over China by weighting each dataset by its uncertainty. Burnett et al
 476 (2020) also used this approach to generate a new rainfall product for the Congo River Basin.
 477 Such an approach was also proposed as a possible way forward by the WATER Cycle Multi-
 478 mission Observation Strategy (WACMOS) project, with the specific suggestion that ET datasets
 479 could be combined on a per-biome scale, if some datasets are known to perform better or
 480 worse under specific conditions (Miralles et al., 2016). However, this approach has the
 481 disadvantage of obscuring the individual problems with each dataset (Miralles et al., 2016). It
 482 may also perturb the larger-scale spatial patterns of ET. Additionally, knowledge of the
 483 individual product errors must be well known so that uncertainty propagation and weighting is
 484 possible. Given that the validity of the assumptions behind triple collocation are not fully
 485 known, any such effort would benefit from additional corroboration of the estimated
 486 uncertainties.

487

488 **4.2. Do spatial patterns in SFE performance match our expectation?**

489 We find that the performance of SFE is not more sensitive to biogeographical gradients than
 490 that of other datasets, suggesting that the simplicity of SFE does not exacerbate performance
 491 issues for specific climate, vegetation, or topographical environments. This is particularly
 492 surprising given the previously hypothesized limitation of SFE in coastal regions, where
 493 atmospheric conditions strongly depend on the influence of the ocean as well as on recent land
 494 fluxes (McColl and Rigden, 2020). However, the SFE method has not previously been applied
 495 within 250 km of the coast, let alone had its errors characterized in these regions. Therefore,
 496 the actual performance of SFE in coastal regions has previously remained unknown.

497 While our statistical analysis (Figure 7, Figure 8) shows the expected increase in SFE σ_e
 498 and reduction in R_T near the coast, particularly within the first four pixels (~20 km), this
 499 behavior is also true for ERA5-Land, which has even more severe performance decreases near
 500 the coast than SFE. This is despite the improved simulation of land surface temperature and
 501 surface energy fluxes in ERA5-Land compared ERA5 for coastal regions, which has been mainly
 502 attributed to ERA5-Land's finer spatial resolution (Martens et al., 2020; Muñoz-Sabater et al.,
 503 2021). However, ERA5-Land performance is not uniformly degraded for all coastal areas (Figure
 504 3). Instead, coastal areas in the North show higher σ_e and R_T compared to coastal areas in the
 505 Southwest and Southeast. This might suggest that the statistically lower performance of ERA5-



Land with coastal proximity in general is due to cross correlation with other climatic factors. Despite the decreased performance of SFE and ERA5-Land near the coast, however, the absolute magnitude of σ_e and R_T for both datasets is still comparable to those of the other datasets throughout the range of coastal proximities, particularly for σ_e . Therefore, coastal proximity may not necessarily limit the usefulness of SFE near coasts. Future SFE implementation and evaluation studies should further investigate these limitations and not exclude areas within 250 km of the coast *a priori*.

SFE has the highest σ_e at low elevations, as does GLEAM and FluxCom. Spatially, however, topographical gradients (such as around the Rocky Mountains) are not apparent on maps of σ_e for any of the datasets (Figure 3), although several smaller mountain ranges (e.g. the Sierra Nevada in California and the upper Appalachian Mountains) do show lower performance for the R_T of SFE and FluxCom. This lack of coherence between the elevation trends and spatial patterns could indicate cross correlation between elevation and other factors impacting performance, which require further investigation.

The most obvious spatial trend in dataset performance is the gradient of performance between the Eastern and Western US. Contrary to expectation, SFE and FluxCom have lower σ_e in the Western US than in the East. One possible explanation for our results is that ET amounts are lower in the West, where vegetation cover is in general lower and aridity higher, such that the overall magnitudes of σ_e are also lower. This would also explain the lack of systematic difference in FluxCom and SFE R_T in the East vs the West. Another explanation might be that SFE and FluxCom both have the highest performance (for both low σ_e and high R_T) in shrublands and grassland land cover types, both of which are often found in the Western US (Dewitz, 2024). This finding is in contrast to Zhu et al. (2024), who found that daily and monthly SFE had the lowest correlation and highest root mean squared error at the eight towers in shrublands, relative to towers in other land covers.

531

532 **4.3. The benefits and limitations of triple collocation**

Triple collocation makes several assumptions, including that the random errors between the datasets are independent, that the random errors are stationary across time, and that the random errors can be described linearly. The assumptions of triple collocation are also implicitly made by more standard validation analyses such as comparison via RMSE (Gruber et al., 2016). However, these assumptions are expected to be violated to some degree, regardless of how carefully comparison datasets are chosen. One reason for this is that most ET models contain at least some overlapping input data, for example the commonly used MODIS reflectance products for vegetation, such as leaf area index, are used as inputs to FLUXCOM, ERA5-Land, and GLEAM (ECMWF, 2018; Jung et al., 2019; Miralles et al., 2025). Any overlap in model input



542 data reduces the likelihood that the resulting ET estimates will have independent errors. Triple
 543 collocation may also fail or wrongly estimate dataset errors if random error magnitudes vary in
 544 time or are not well described linearly. Therefore, it is not uncommon for triple collocation
 545 studies to have invalid pixel results (e.g. He et al., 2023). Some triple collocation studies also
 546 choose to pre-filter pixels to ensure high correlation coefficient between the raw datasets
 547 (Gruber et al., 2016; McColl et al., 2014), which also leads to pixels where triple collocation
 548 results are missing.

549 One way to increase the confidence in an application of triple collocation is to repeat
 550 the analysis for multiple triplets, as performed here. Violations in the triple collocation
 551 assumptions would lead to differences in the estimated error statistic for a given dataset
 552 depending on which datasets are used for comparison (He et al., 2023; McColl et al., 2014). We
 553 found that invalid triple collocation results were more prevalent when FluxCom and ERA5-Land
 554 were compared within the same triplet, regardless of the third dataset. This suggests that the
 555 assumption of independent errors may be worse between these two datasets, despite their
 556 seemingly larger input difference than GLEAM and FluxCom, for example, which both
 557 incorporate machine learning. Nevertheless, the overall high agreement between different
 558 triple collocation estimates for the other triplets - and the lack of coherent spatial pattern in
 559 error variability across triplets (Figure 5) - strongly increases our confidence that our overall
 560 error estimates are robust.

561 One limitation of triple collocation is that it cannot provide information about
 562 multiplicative dataset biases (β_i) beyond estimating relative biases with reference to one
 563 member of each triplet which is assumed to have no bias (Gruber et al., 2016; McColl et al.,
 564 2014). However, previous work suggests that SFE may have issues with bias particularly along
 565 aridity gradients. For example, Chen et al. (2021) and Zhu et al. (2024) both found that SFE ET
 566 had higher bias in arid conditions and tended to underestimate ET in wet conditions. This same
 567 pattern was also observed for comparisons of in situ SFE to eddy covariance data (McColl and
 568 Rigden, 2020; Thakur et al., 2025). While we do not consider bias because triple collocation only
 569 allows for its calculation relative to a comparison dataset, we do see that SFE σ_e is highest at the
 570 driest and wettest pixels compared to pixels with intermediate mean annual precipitation. SFE
 571 R_T , on the other hand, shows only a weak but slightly decreasing relationship with increasing
 572 mean annual precipitation. Additional investigation into this is necessary. However the problem
 573 of ET overestimation in arid conditions - when surface evaporation is high in general - is not
 574 unique to SFE (McColl and Rigden, 2020; Miralles et al., 2016; Salvucci and Gentile, 2013).
 575 Despite the assumptions and limitations of triple collocation, the method's ability to quantify
 576 error statistics relative to true ET without needing an error-free dataset of ET remains a
 577 substantial and unique benefit.

578



579 **5. Conclusions**

580 SFE allows for observational, data-driven estimates of ET with no tunable parameters or land
 581 surface information required. In leveraging land-atmosphere coupling, SFE estimates ET from
 582 atmospheric conditions alone, and therefore provides an opportunity to test hypotheses about
 583 vegetation response to environmental drivers without assuming that response *a priori* in the
 584 creation of the ET estimate itself. The lack of parameterization for SFE eases issues of circularity
 585 constraining research into essential outstanding challenges in ecohydrology, such as the
 586 response of ET to drought (Zhao et al., 2022) and the inference of subsurface water storage
 587 from changes in vegetation behavior (Dralle et al., 2020; Feldman et al., 2023; Stocker et al.,
 588 2023). Based on triple collocation - and despite its simplicity - SFE exhibits comparable
 589 performance to the more complicated ET estimates from GLEAM, FluxCom, and ERA5-Land.

591 **6. Code availability**

592 Code is available on GitHub at <https://github.com/erica-mccormick/surface-flux-equilibrium>.

594 **7. Data availability**

595 All of the data used to estimate SFE ET as well as the comparison ET datasets are publicly
 596 available online. Daily 4 km estimates of SFE ET across CONUS calculated here from 1979 to
 597 2024 will be made available at Zenodo upon acceptance of the manuscript.

599 **8. Acknowledgments**

600 ELM, LES, and AGK were supported by NSF DEB 1942133. AGK was also supported by the Alfred
 601 P. Sloan Foundation and by the Gordon and Betty Moore Foundation under grant 11974. ELM
 602 was supported by the Stanford University Diversifying Academia Recruiting Excellence Doctoral
 603 Fellowship and by the NSF GRFP. KAM acknowledges funding from NSF grant AGS-2129576, an
 604 NSF CAREER award (AGS-2441565), and a Sloan Research Fellowship (FG-2023-19963).

606 **9. Competing interests**

607 The authors declare that they have no conflict of interest.

609 **10. References**

610 Abatzoglou, J. T.: Development of gridded surface meteorological data for ecological
 611 applications and modelling, *Int. J. Climatol.*, 33, 121–131,
 612 <https://doi.org/10.1002/joc.3413>, 2013.



- 613 ArcGIS Data and Maps: USA Detailed Water Bodies, 2023.
- 614 Beven, K. J. and Kirkby, M. J.: A physically-based, variable contributing area model of basin
 615 hydrology, *Hydrol. Sci. Bull.*, 24, 43–69, <https://doi.org/10.1080/02626667909491834>,
 616 1979.
- 617 Burnett, M. W., Quetin, G. R., and Konings, A. G.: Data-driven estimates of evapotranspiration
 618 and its controls in the Congo Basin, *Hydrol. Earth Syst. Sci.*, 24, 4189–4211,
 619 <https://doi.org/10.5194/hess-24-4189-2020>, 2020.
- 620 Chen, F., Crow, W. T., Bindlish, R., Colliander, A., Burgin, M. S., Asanuma, J., and Aida, K.:
 621 Global-scale evaluation of SMAP, SMOS and ASCAT soil moisture products using triple
 622 collocation, *Remote Sens. Environ.*, 214, 1–13, <https://doi.org/10.1016/j.rse.2018.05.008>,
 623 2018.
- 624 Chen, S., McColl, K. A., Berg, A., and Huang, Y.: Surface Flux Equilibrium Estimates of
 625 Evapotranspiration at Large Spatial Scales, *J. Hydrometeorol.*, 22, 765–779,
 626 <https://doi.org/10.1175/JHM-D-20-0204.1>, 2021.
- 627 Crow, W. T., Lei, F., Hain, C., Anderson, M. C., Scott, R. L., Billesbach, D., and Arkebauer, T.:
 628 Robust estimates of soil moisture and latent heat flux coupling strength obtained from
 629 triple collocation: ESTIMATION OF LAND COUPLING STRENGTH, *Geophys. Res. Lett.*, 42,
 630 8415–8423, <https://doi.org/10.1002/2015GL065929>, 2015.
- 631 Dewitz: National Land Cover Database (NLCD) 2019 Products (ver. 3.0, February 2024),
 632 <https://doi.org/10.5066/P9KZCM54>, 2024.
- 633 Doelling, D. R., Loeb, N. G., Keyes, D. F., Nordeen, M. L., Morstad, D., Nguyen, C., Wielicki, B.
 634 A., Young, D. F., and Sun, M.: Geostationary Enhanced Temporal Interpolation for CERES
 635 Flux Products, *J. Atmospheric Ocean. Technol.*, 30, 1072–1090,
 636 <https://doi.org/10.1175/JTECH-D-12-00136.1>, 2013.
- 637 Dralle, D. N., Hahm, W. J., Chadwick, K. D., McCormick, E. L., and Rempe, D. M.: Technical note:
 638 Accounting for snow in the estimation of root-zone water storage capacity from
 639 precipitation and evapotranspiration fluxes, *Hydrol. Earth Syst. Sci.*, 1–9,
 640 <https://doi.org/10.5194/hess-2020-602>, 2020.
- 641 Draper, C., Reichle, R., De Jeu, R., Naeimi, V., Parinussa, R., and Wagner, W.: Estimating root
 642 mean square errors in remotely sensed soil moisture over continental scale domains,
 643 *Remote Sens. Environ.*, 137, 288–298, <https://doi.org/10.1016/j.rse.2013.06.013>, 2013.
- 644 ECMWF: IFS Documentation CY45R1 - Part IV : Physical processes,
 645 <https://doi.org/10.21957/4WHWO8JW0>, 2018.
- 646 Entekhabi, D., Reichle, R. H., Koster, R. D., and Crow, W. T.: Performance Metrics for Soil
 647 Moisture Retrievals and Application Requirements, *J. Hydrometeorol.*, 11, 832–840,



- 648 <https://doi.org/10.1175/2010JHM1223.1>, 2010.
- 649 Eyring, V., Bony, S., Meehl, G. A., Senior, C. A., Stevens, B., Stouffer, R. J., and Taylor, K. E.:
 650 Overview of the Coupled Model Intercomparison Project Phase 6 (CMIP6) experimental
 651 design and organization, *Geosci. Model Dev.*, 9, 1937–1958, [https://doi.org/10.5194/gmd-](https://doi.org/10.5194/gmd-9-1937-2016)
 652 9-1937-2016, 2016.
- 653 Feldman, A. F., Short Gianotti, D. J., Dong, J., Akbar, R., Crow, W. T., McColl, K. A., Konings, A.
 654 G., Nippert, J. B., Tumber-Dávila, S. J., Holbrook, N. M., Rockwell, F. E., Scott, R. L., Reichle,
 655 R. H., Chatterjee, A., Joiner, J., Poulter, B., and Entekhabi, D.: Remotely Sensed Soil
 656 Moisture Can Capture Dynamics Relevant to Plant Water Uptake, *Water Resour. Res.*, 59,
 657 e2022WR033814, <https://doi.org/10.1029/2022WR033814>, 2023.
- 658 Ferreira, V. G., Montecino, H. D. C., Yakubu, C. I., and Heck, B.: Uncertainties of the Gravity
 659 Recovery and Climate Experiment time-variable gravity-field solutions based on three-
 660 cornered hat method, *J. Appl. Remote Sens.*, 10, 015015,
 661 <https://doi.org/10.1117/1.JRS.10.015015>, 2016.
- 662 Fisher, J. B., Lee, B., Purdy, A. J., Halverson, G. H., Dohlen, M. B., Cawse-Nicholson, K., Wang,
 663 A., Anderson, R. G., Aragon, B., Arain, M. A., Baldocchi, D. D., Baker, J. M., Barral, H.,
 664 Bernacchi, C. J., Bernhofer, C., Biraud, S. C., Bohrer, G., Brunsell, N., Cappelaere, B., Castro-
 665 Contreras, S., Chun, J., Conrad, B. J., Cremonese, E., Demarty, J., Desai, A. R., De Ligne, A.,
 666 Foltýnová, L., Goulden, M. L., Griffis, T. J., Grünwald, T., Johnson, M. S., Kang, M., Kelbe, D.,
 667 Kowalska, N., Lim, J., Mainassara, I., McCabe, M. F., Missik, J. E. C., Mohanty, B. P., Moore,
 668 C. E., Morillas, L., Morrison, R., Munger, J. W., Posse, G., Richardson, A. D., Russell, E. S.,
 669 Ryu, Y., Sanchez-Azofeifa, A., Schmidt, M., Schwartz, E., Sharp, I., Šigut, L., Tang, Y., Hulley,
 670 G., Anderson, M., Hain, C., French, A., Wood, E., and Hook, S.: ECOSTRESS: NASA's Next
 671 Generation Mission to Measure Evapotranspiration From the International Space Station,
 672 *Water Resour. Res.*, 56, e2019WR026058, <https://doi.org/10.1029/2019WR026058>, 2020.
- 673 Friedlingstein, P., Jones, M. W., O'Sullivan, M., Andrew, R. M., Hauck, J., Peters, G. P., Peters,
 674 W., Pongratz, J., Sitch, S., Le Quéré, C., Bakker, D. C. E., Canadell, J. G., Ciais, P., Jackson, R.
 675 B., Anthoni, P., Barbero, L., Bastos, A., Bastrikov, V., Becker, M., Bopp, L., Buitenhuis, E.,
 676 Chandra, N., Chevallier, F., Chini, L. P., Currie, K. I., Feely, R. A., Gehlen, M., Gilfillan, D.,
 677 Gkritzalis, T., Goll, D. S., Gruber, N., Gutekunst, S., Harris, I., Haverd, V., Houghton, R. A.,
 678 Hurtt, G., Ilyina, T., Jain, A. K., Joetzjer, E., Kaplan, J. O., Kato, E., Klein Goldewijk, K.,
 679 Korsbakken, J. I., Landschützer, P., Lauvset, S. K., Lefèvre, N., Lenton, A., Lienert, S.,
 680 Lombardozi, D., Marland, G., McGuire, P. C., Melton, J. R., Metzl, N., Munro, D. R., Nabel,
 681 J. E. M. S., Nakaoka, S.-I., Neill, C., Omar, A. M., Ono, T., Peregón, A., Pierrot, D., Poulter, B.,
 682 Rehder, G., Resplandy, L., Robertson, E., Rödenbeck, C., Séférian, R., Schwinger, J., Smith,
 683 N., Tans, P. P., Tian, H., Tilbrook, B., Tubiello, F. N., van der Werf, G. R., Wiltshire, A. J., and
 684 Zaehle, S.: Global Carbon Budget 2019, *Earth Syst. Sci. Data*, 11, 1783–1838,
 685 <https://doi.org/10.5194/essd-11-1783-2019>, 2019.
- 686 Good, S. P., Noone, D., and Bowen, G.: Hydrologic connectivity constrains partitioning of global



- 687 terrestrial water fluxes, *Science*, 349, 175–177, <https://doi.org/10.1126/science.aaa5931>,
 688 2015.
- 689 Green, J. K., Konings, A. G., Alemohammad, S. H., Berry, J., Entekhabi, D., Kolassa, J., Lee, J.-E.,
 690 and Gentine, P.: Regionally strong feedbacks between the atmosphere and terrestrial
 691 biosphere, *Nat. Geosci.*, 10, 410–414, <https://doi.org/10.1038/ngeo2957>, 2017.
- 692 Gruber, A., Su, C.-H., Zwieback, S., Crow, W., Dorigo, W., and Wagner, W.: Recent advances in
 693 (soil moisture) triple collocation analysis, *Int. J. Appl. Earth Obs. Geoinformation*, 45, 200–
 694 211, <https://doi.org/10.1016/j.jag.2015.09.002>, 2016.
- 695 He, Y., Wang, C., Hu, J., Mao, H., Duan, Z., Qu, C., Li, R., Wang, M., and Song, X.: Discovering
 696 Optimal Triplets for Assessing the Uncertainties of Satellite-Derived Evapotranspiration
 697 Products, *Remote Sens.*, 15, 3215, <https://doi.org/10.3390/rs15133215>, 2023.
- 698 Hersbach, H., Bell, B., Berrisford, P., Hirahara, S., Horányi, A., Muñoz-Sabater, J., Nicolas, J.,
 699 Peubey, C., Radu, R., Schepers, D., Simmons, A., Soci, C., Abdalla, S., Abellan, X., Balsamo,
 700 G., Bechtold, P., Biavati, G., Bidlot, J., Bonavita, M., De Chiara, G., Dahlgren, P., Dee, D.,
 701 Diamantakis, M., Dragani, R., Flemming, J., Forbes, R., Fuentes, M., Geer, A., Haimberger,
 702 L., Healy, S., Hogan, R. J., Hólm, E., Janisková, M., Keeley, S., Laloyaux, P., Lopez, P., Lupu,
 703 C., Radnoti, G., De Rosnay, P., Rozum, I., Vamborg, F., Villaume, S., and Thépaut, J.: The
 704 ERA5 global reanalysis, *Q. J. R. Meteorol. Soc.*, 146, 1999–2049,
 705 <https://doi.org/10.1002/qj.3803>, 2020.
- 706 Jung, M., Koirala, S., Weber, U., Ichii, K., Gans, F., Camps-Valls, G., Papale, D., Schwalm, C.,
 707 Tramontana, G., and Reichstein, M.: The FLUXCOM ensemble of global land-atmosphere
 708 energy fluxes, *Sci. Data*, 6, 74, <https://doi.org/10.1038/s41597-019-0076-8>, 2019.
- 709 Koppa, A., Rains, D., Hulsman, P., Poyatos, R., and Miralles, D. G.: A deep learning-based hybrid
 710 model of global terrestrial evaporation, *Nat. Commun.*, 13, 1912,
 711 <https://doi.org/10.1038/s41467-022-29543-7>, 2022.
- 712 Martens, B., Miralles, D. G., Lievens, H., Van Der Schalie, R., De Jeu, R. A. M., Fernández-Prieto,
 713 D., Beck, H. E., Dorigo, W. A., and Verhoest, N. E. C.: GLEAM v3: satellite-based land
 714 evaporation and root-zone soil moisture, *Geosci. Model Dev.*, 10, 1903–1925,
 715 <https://doi.org/10.5194/gmd-10-1903-2017>, 2017.
- 716 Martens, B., Schumacher, D. L., Wouters, H., Muñoz-Sabater, J., Verhoest, N. E. C., and
 717 Miralles, D. G.: Evaluating the land-surface energy partitioning in ERA5, *Geosci. Model*
 718 *Dev.*, 13, 4159–4181, <https://doi.org/10.5194/gmd-13-4159-2020>, 2020.
- 719 McColl, K. A. and Rigden, A. J.: Emergent Simplicity of Continental Evapotranspiration,
 720 *Geophys. Res. Lett.*, 47, <https://doi.org/10.1029/2020GL087101>, 2020.
- 721 McColl, K. A., Vogelzang, J., Konings, A. G., Entekhabi, D., Piles, M., and Stoffelen, A.: Extended
 722 triple collocation: Estimating errors and correlation coefficients with respect to an



- 723 unknown target, *Geophys. Res. Lett.*, 41, 6229–6236,
 724 <https://doi.org/10.1002/2014GL061322>, 2014.
- 725 McColl, K. A., Salvucci, G. D., and Gentine, P.: Surface Flux Equilibrium Theory Explains an
 726 Empirical Estimate of Water-Limited Daily Evapotranspiration, *J. Adv. Model. Earth Syst.*,
 727 11, 2036–2049, <https://doi.org/10.1029/2019MS001685>, 2019.
- 728 Mesinger, F., DiMego, G., Kalnay, E., Mitchell, K., Shafran, P. C., Ebisuzaki, W., Jović, D.,
 729 Woollen, J., Rogers, E., Berbery, E. H., Ek, M. B., Fan, Y., Grumbine, R., Higgins, W., Li, H.,
 730 Lin, Y., Manikin, G., Parrish, D., and Shi, W.: North American Regional Reanalysis, *Bull. Am.*
 731 *Meteorol. Soc.*, 87, 343–360, <https://doi.org/10.1175/BAMS-87-3-343>, 2006.
- 732 Miralles, D. G., Crow, W. T., and Cosh, M. H.: Estimating Spatial Sampling Errors in Coarse-Scale
 733 Soil Moisture Estimates Derived from Point-Scale Observations, *J. Hydrometeorol.*, 11,
 734 1423–1429, <https://doi.org/10.1175/2010JHM1285.1>, 2010.
- 735 Miralles, D. G., Holmes, T. R. H., De Jeu, R. A. M., Gash, J. H., Meesters, A. G. C. A., and Dolman,
 736 A. J.: Global land-surface evaporation estimated from satellite-based observations, *Hydrol.*
 737 *Earth Syst. Sci.*, 15, 453–469, <https://doi.org/10.5194/hess-15-453-2011>, 2011.
- 738 Miralles, D. G., Jiménez, C., Jung, M., Michel, D., Ershadi, A., McCabe, M. F., Hirschi, M.,
 739 Martens, B., Dolman, A. J., Fisher, J. B., Mu, Q., Seneviratne, S. I., Wood, E. F., and
 740 Fernández-Prieto, D.: The WACMOS-ET project – Part 2: Evaluation of global terrestrial
 741 evaporation data sets, *Hydrol. Earth Syst. Sci.*, 20, 823–842, [https://doi.org/10.5194/hess-](https://doi.org/10.5194/hess-20-823-2016)
 742 20-823-2016, 2016.
- 743 Miralles, D. G., Bonte, O., Koppa, A., Baez-Villanueva, O. M., Tronquo, E., Zhong, F., Beck, H. E.,
 744 Hulsman, P., Dorigo, W., Verhoest, N. E. C., and Haghdoust, S.: GLEAM4: global land
 745 evaporation and soil moisture dataset at 0.1° resolution from 1980 to near present, *Sci.*
 746 *Data*, 12, 416, <https://doi.org/10.1038/s41597-025-04610-y>, 2025.
- 747 Mu, Q., Zhao, M., and Running, S. W.: Improvements to a MODIS global terrestrial
 748 evapotranspiration algorithm, *Remote Sens. Environ.*, 115, 1781–1800,
 749 <https://doi.org/10.1016/j.rse.2011.02.019>, 2011.
- 750 Muñoz-Sabater, J., Dutra, E., Agustí-Panareda, A., Albergel, C., Arduini, G., Balsamo, G.,
 751 Boussetta, S., Choulga, M., Harrigan, S., Hersbach, H., Martens, B., Miralles, D. G., Piles, M.,
 752 Rodríguez-Fernández, N. J., Zsoter, E., Buontempo, C., and Thépaut, J.-N.: ERA5-Land: a
 753 state-of-the-art global reanalysis dataset for land applications, *Earth Syst. Sci. Data*, 13,
 754 4349–4383, <https://doi.org/10.5194/essd-13-4349-2021>, 2021.
- 755 Oki, T. and Kanae, S.: Global Hydrological Cycles and World Water Resources, *Freshw. Resour.*,
 756 313, 5, 2006.
- 757 Salvucci, G. D. and Gentine, P.: Emergent relation between surface vapor conductance and
 758 relative humidity profiles yields evaporation rates from weather data, *Proc. Natl. Acad. Sci.*,



- 759 110, 6287–6291, <https://doi.org/10.1073/pnas.1215844110>, 2013.
- 760 Savoca, M. E., Senay, G. B., Maupin, M. A., Kenny, J. F., and Perry, C. A.: Actual
 761 evapotranspiration modeling using the operational Simplified Surface Energy Balance
 762 (SSEBop) approach, Reston, VA, <https://doi.org/10.3133/sir20135126>, 2013.
- 763 Scipal, K., Holmes, T., De Jeu, R., Naeimi, V., and Wagner, W.: A possible solution for the
 764 problem of estimating the error structure of global soil moisture data sets, *Geophys. Res.*
 765 *Lett.*, 35, <https://doi.org/10.1029/2008gl035599>, 2008.
- 766 Stocker, B. D., Tumber-Dávila, S. J., Konings, A. G., Anderson, M. C., Hain, C., and Jackson, R. B.:
 767 Global patterns of water storage in the rooting zones of vegetation, *Nat. Geosci.*, 16, 250–
 768 256, <https://doi.org/10.1038/s41561-023-01125-2>, 2023.
- 769 Stoffelen, A.: Toward the true near-surface wind speed: Error modeling and calibration using
 770 triple collocation, *J. Geophys. Res. Oceans*, 103, 7755–7766,
 771 <https://doi.org/10.1029/97JC03180>, 1998.
- 772 Sun, J., McColl, K. A., Wang, Y., Rigden, A. J., Lu, H., Yang, K., Li, Y., and Santanello, J. A.: Global
 773 evaluation of terrestrial near-surface air temperature and specific humidity retrievals from
 774 the Atmospheric Infrared Sounder (AIRS), *Remote Sens. Environ.*, 252, 112146,
 775 <https://doi.org/10.1016/j.rse.2020.112146>, 2021.
- 776 Teuling, A. J., Seneviratne, S. I., Stöckli, R., Reichstein, M., Moors, E., Ciais, P., Luyssaert, S., Van
 777 Den Hurk, B., Ammann, C., Bernhofer, C., Dellwik, E., Gianelle, D., Gielen, B., Grünwald, T.,
 778 Klumpp, K., Montagnani, L., Moureaux, C., Sottocornola, M., and Wohlfahrt, G.:
 779 Contrasting response of European forest and grassland energy exchange to heatwaves,
 780 *Nat. Geosci.*, 3, 722–727, <https://doi.org/10.1038/ngeo950>, 2010.
- 781 Thakur, H., Raghav, P., Kumar, M., and Wolkeba, F.: Surface Flux Equilibrium Theory-Derived
 782 Evapotranspiration Estimate Outperforms ECOSTRESS, MODIS, and SSEBop Products,
 783 *Geophys. Res. Lett.*, 52, e2025GL114822, <https://doi.org/10.1029/2025GL114822>, 2025.
- 784 United States Census Bureau: TIGER/Line Shapefile, 2019, nation, U.S., Coastline National
 785 Shapefile, 2019.
- 786 Xia, Y., Mitchell, K., Ek, M., Sheffield, J., Cosgrove, B., Wood, E., Luo, L., Alonge, C., Wei, H.,
 787 Meng, J., Livneh, B., Lettenmaier, D., Koren, V., Duan, Q., Mo, K., Fan, Y., and Mocko, D.:
 788 Continental-scale water and energy flux analysis and validation for the North American
 789 Land Data Assimilation System project phase 2 (NLDAS-2): 1. Intercomparison and
 790 application of model products, *J. Geophys. Res. Atmospheres*, 117, 2011JD016048,
 791 <https://doi.org/10.1029/2011JD016048>, 2012.
- 792 Yamazaki, D., Ikeshima, D., Sosa, J., Bates, P. D., Allen, G. H., and Pavelsky, T. M.: MERIT Hydro:
 793 A High-Resolution Global Hydrography Map Based on Latest Topography Dataset, *Water*
 794 *Resour. Res.*, 55, 5053–5073, <https://doi.org/10.1029/2019WR024873>, 2019.



- 795 Yang, Y., Roderick, M. L., Guo, H., Miralles, D. G., Zhang, L., Fatichi, S., Luo, X., Zhang, Y.,
 796 McVicar, T. R., Tu, Z., Keenan, T. F., Fisher, J. B., Gan, R., Zhang, X., Piao, S., Zhang, B., and
 797 Yang, D.: Evapotranspiration on a greening Earth, *Nat. Rev. Earth Environ.*, 4, 626–641,
 798 <https://doi.org/10.1038/s43017-023-00464-3>, 2023.
- 799 Yilmaz, M. T. and Crow, W. T.: Evaluation of Assumptions in Soil Moisture Triple Collocation
 800 Analysis, *J. Hydrometeorol.*, 15, 1293–1302, <https://doi.org/10.1175/JHM-D-13-0158.1>,
 801 2014.
- 802 Yin, X., Jiang, B., Liang, S., Li, S., Zhao, X., Wang, Q., Xu, J., Han, J., Liang, H., Zhang, X., Liu, Q.,
 803 Yao, Y., Jia, K., and Xie, X.: Significant discrepancies of land surface daily net radiation
 804 among ten remotely sensed and reanalysis products, *Int. J. Digit. Earth*, 16, 3725–3752,
 805 <https://doi.org/10.1080/17538947.2023.2253211>, 2023.
- 806 Zhao, M., A. G., Liu, Y., and Konings, A. G.: Evapotranspiration frequently increases during
 807 droughts, *Nat. Clim. Change*, 12, 1024–1030, <https://doi.org/10.1038/s41558-022-01505-3>,
 808 2022.
- 809 Zhu, W., Yu, X., Wei, J., and Lv, A.: Surface flux equilibrium estimates of evaporative fraction
 810 and evapotranspiration at global scale: Accuracy evaluation and performance comparison,
 811 *Agric. Water Manag.*, 291, 108609, <https://doi.org/10.1016/j.agwat.2023.108609>, 2024.